Electronic Supplementary Material (ESI) for New Journal of Chemistry.

Supplementary Materials

Engineering hierarchical manganese molybdenum sulfide nanosheets integrated cathode for high-energy density hybrid supercapacitors

Chao Li,[a,b] Qiong Liu,[a] Lu Liu,[a] Ge Wu,[a] Yulong Zhang,[a] Sihan Liu,[a] Ruhua Zha,[a,b] Yu Zhang,*[a,b] Qing Li*[a,b]

[a] College of Chemistry and Chemical Engineering, Xinyang Normal University, Xinyang 464000, China

[b] Xinyang Key Laboratory of Low-Carbon Energy Materials, Xinyang Normal University, Xinyang 464000, China

*Corresponding authors.

E-mail addresses: yuzhang@xynu.edu.cn; lqlq0312@163.com.

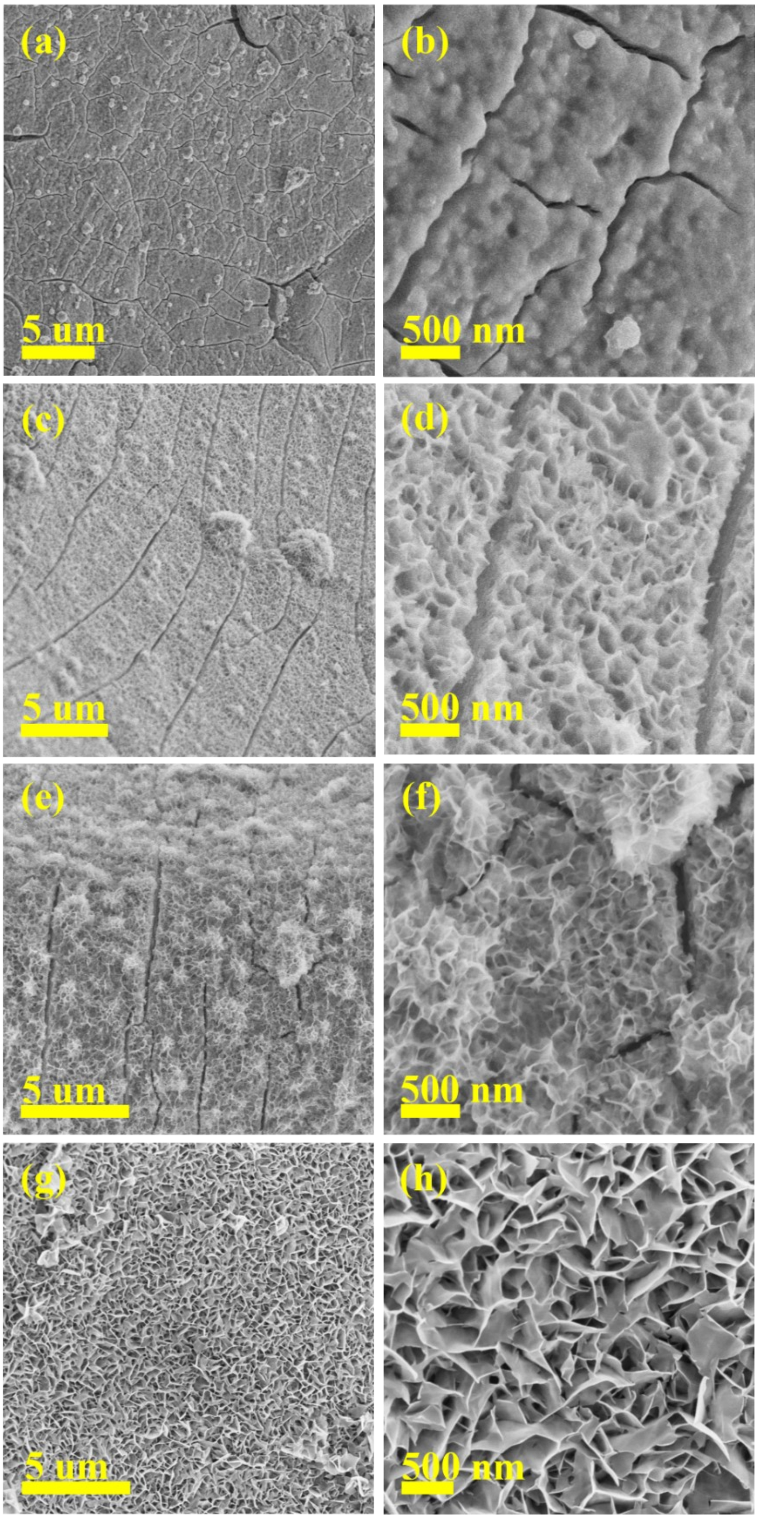

Fig.S1. Low- and high-magnification SEM images for $MnMoO_4 \cdot H_2O$ NSs by performing the hydrothermal reactions for 2-8h; (a) and (b) for $MnMoO_4 \cdot H_2O$ NSs-2; (c) and (d) for $MnMoO_4 \cdot H_2O$ NSs-4; (e) and (f) for $MnMoO_4 \cdot H_2O$ NSs-6; (g) and (h) for $MnMoO_4 \cdot H_2O$ NSs-8.

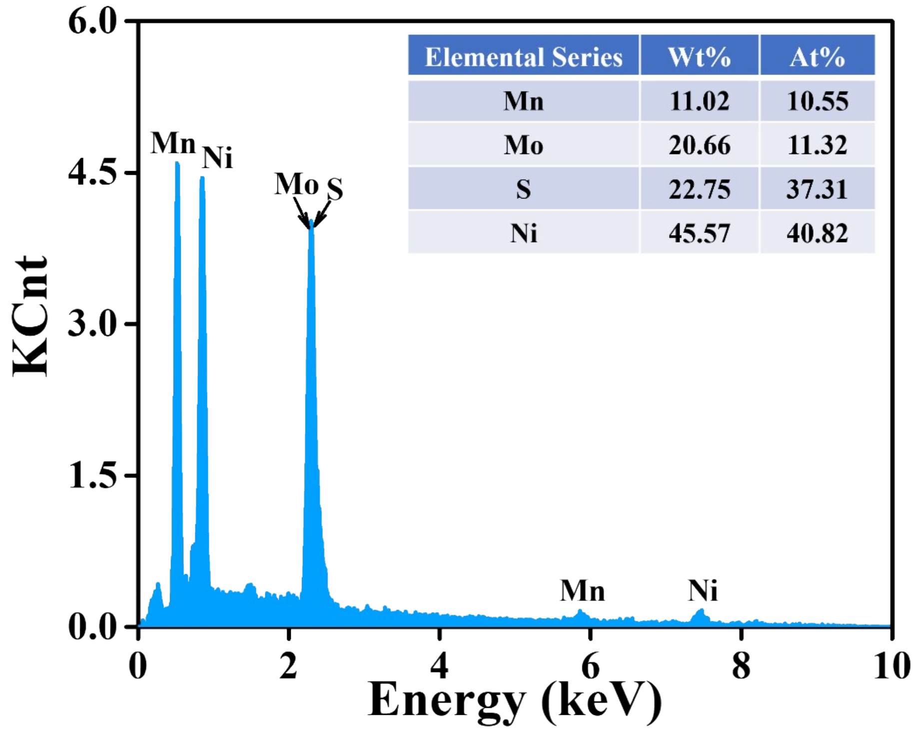

Fig.S2. EDAX spectrum for Mn-Mo-S NSs.

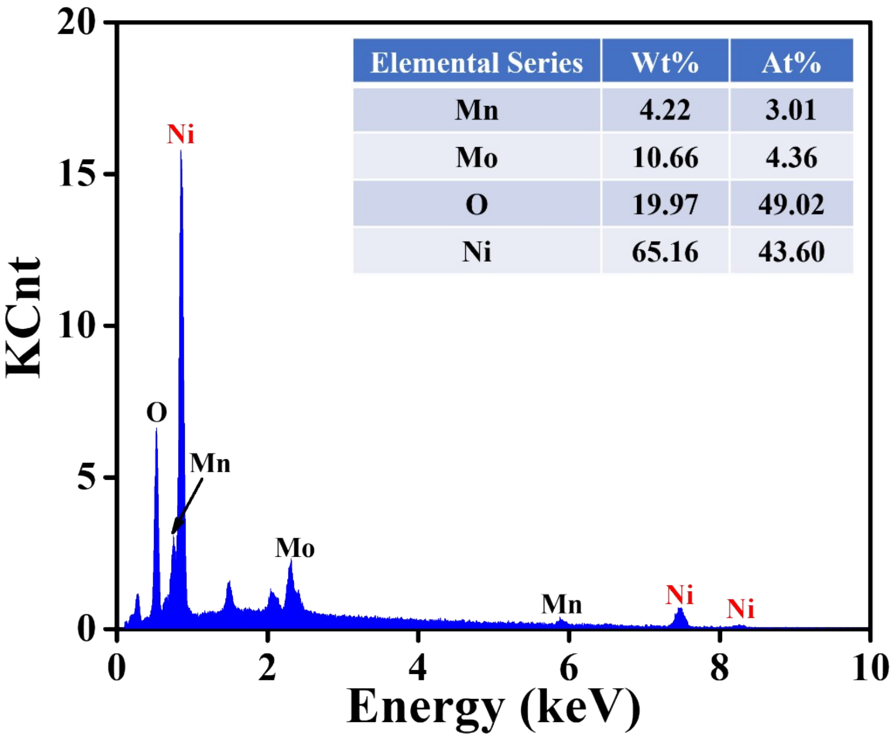

Elemental Series	Wt%	At%
Mn	4.22	3.01
Mo	10.66	4.36
O	19.97	49.02
Ni	65.16	43.60

Fig.S3. EDAX spectrum for $MnMoO_4{\cdot}H_2O$ NSs-8.

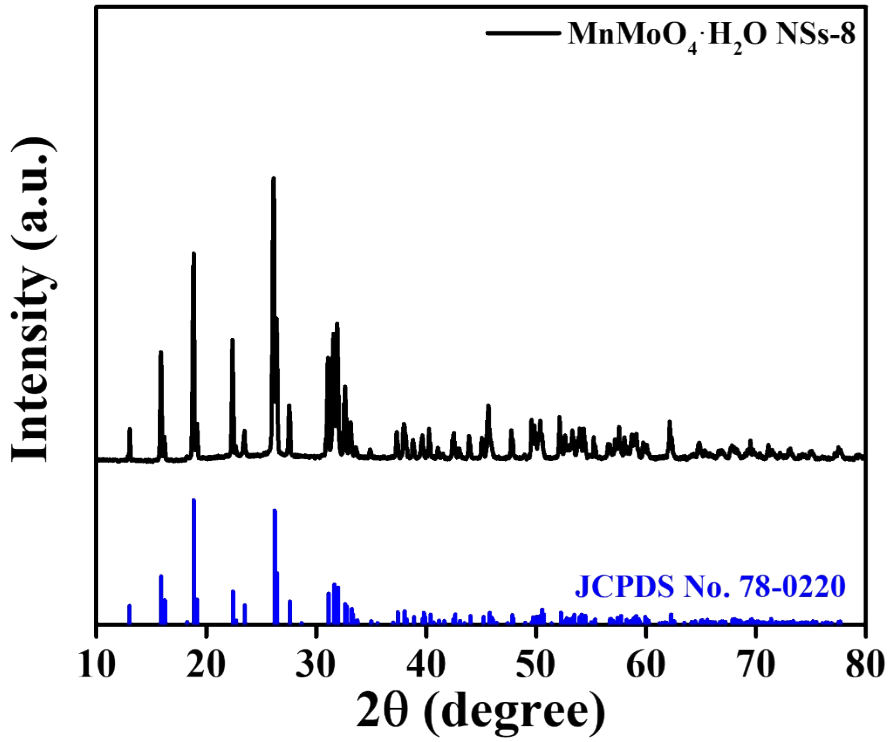

Fig.S4. XRD pattern for $MnMoO_4 \cdot H_2O$ NSs-8.

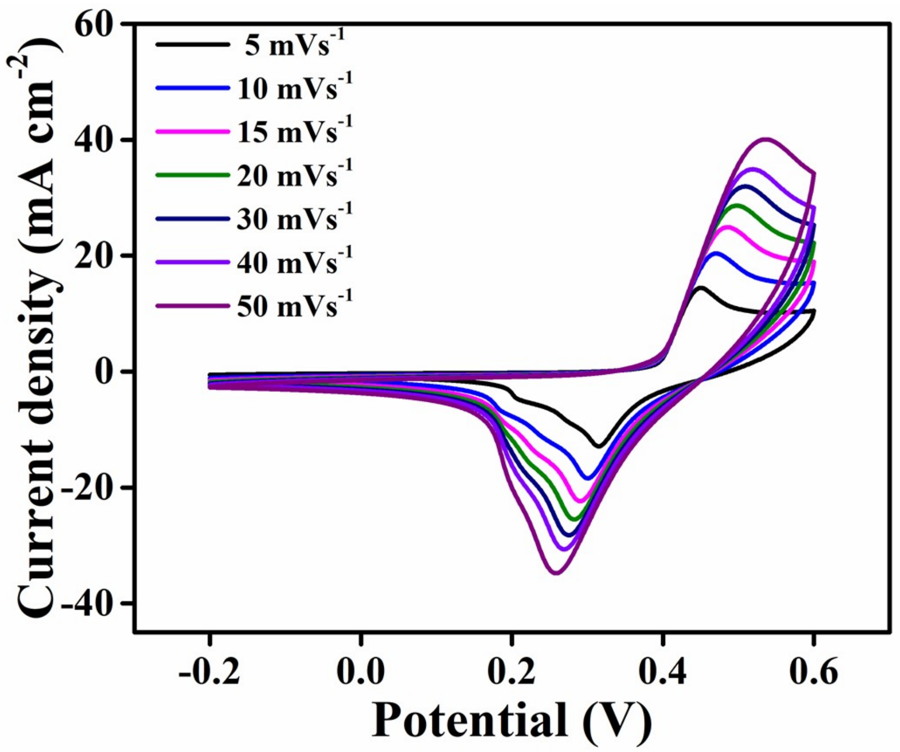

Fig.S5. CV curves for $MnMoO_4 \cdot H_2O$ NSs-8.

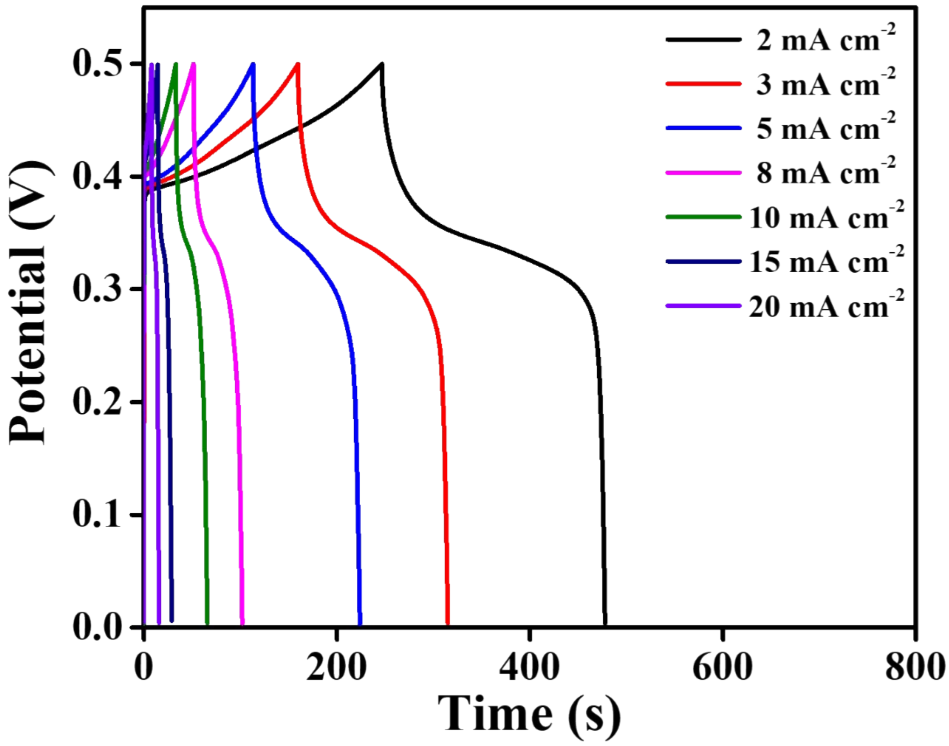

Fig.S6. GCD curves for $MnMoO_4 \cdot H_2O$ NSs-8.

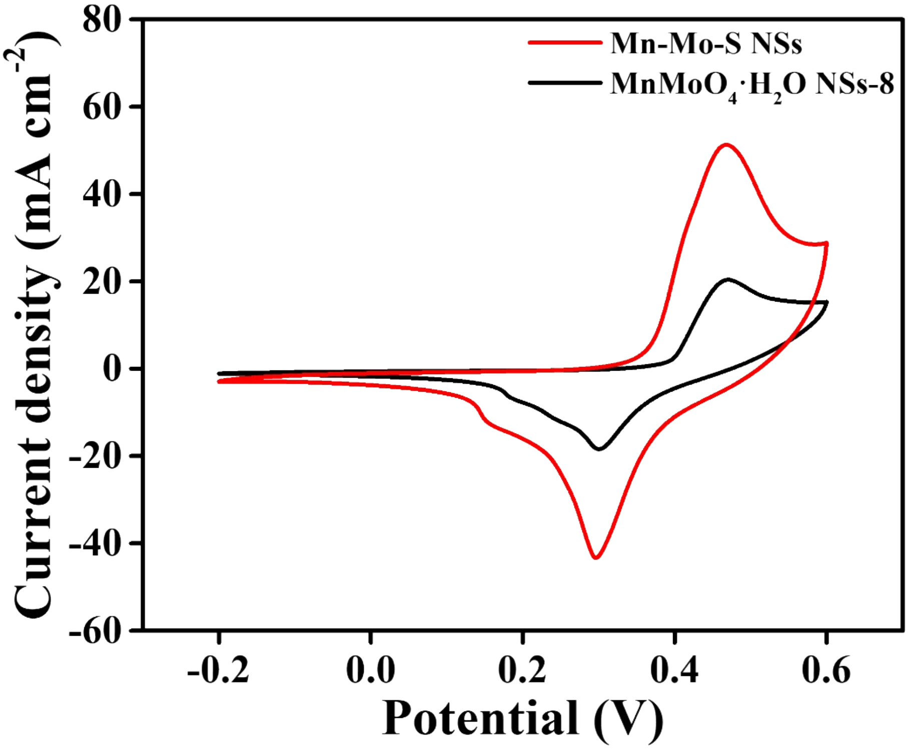

Fig.S7. CV curves comparison of Mn-Mo-S NSs and $MnMoO_4 \cdot H_2O$ NSs-8 at 10 mV s^{-1}.

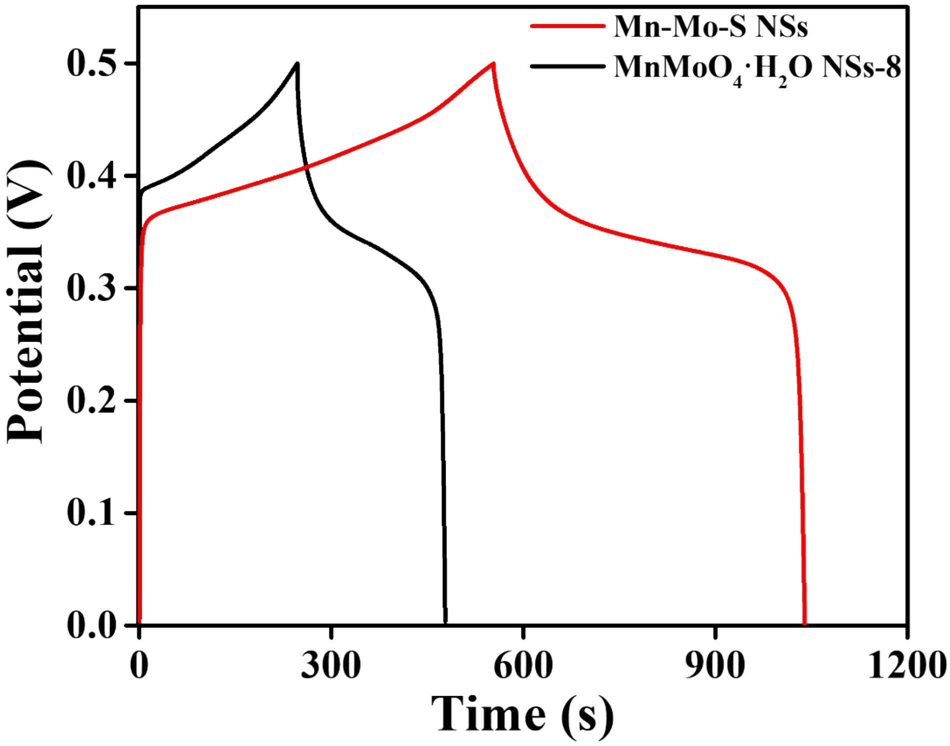

Fig.S8. GCD curves comparison of Mn-Mo-S NSs and $MnMoO_4 \cdot H_2O$ NSs-8 at 2 mA cm^{-2}.

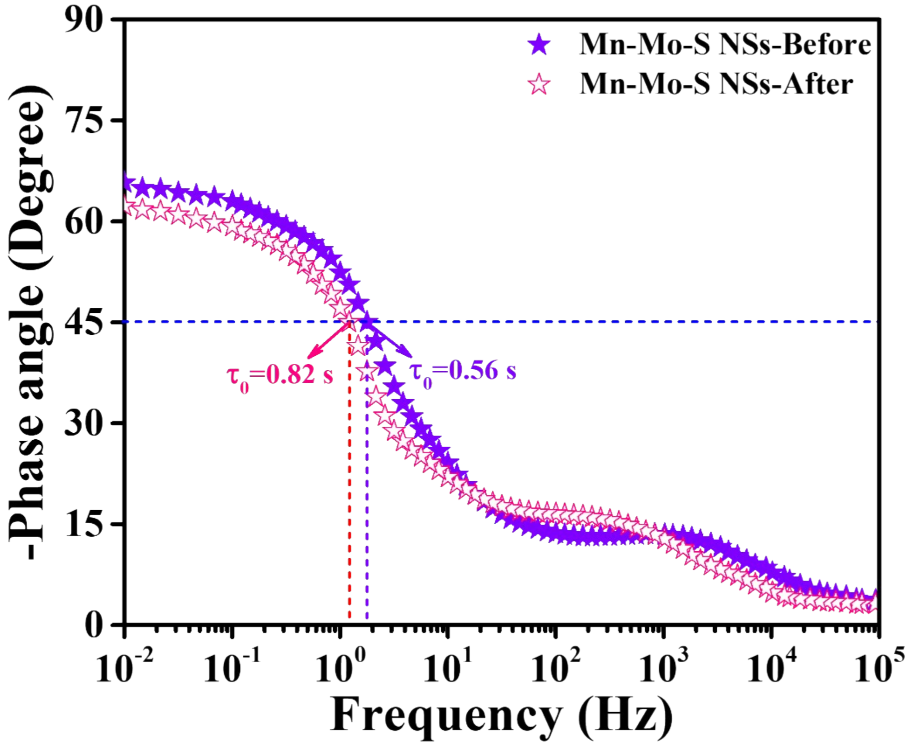

Fig.S9. Bode phase angle plots of Mn-Mo-S NSs-Before and Mn-Mo-S NSs-After.

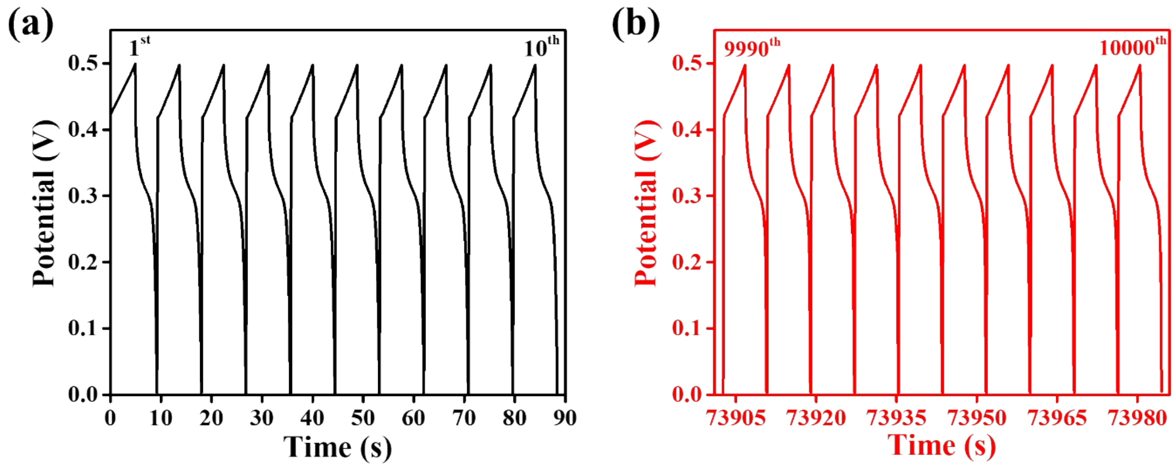

Fig.S10. The initial and final 10 GCD cycles for Mn-Mo-S NSs integrated cathode in the cyclic stability test at 50 mA cm^{-2} for 10000 GCD cycles.

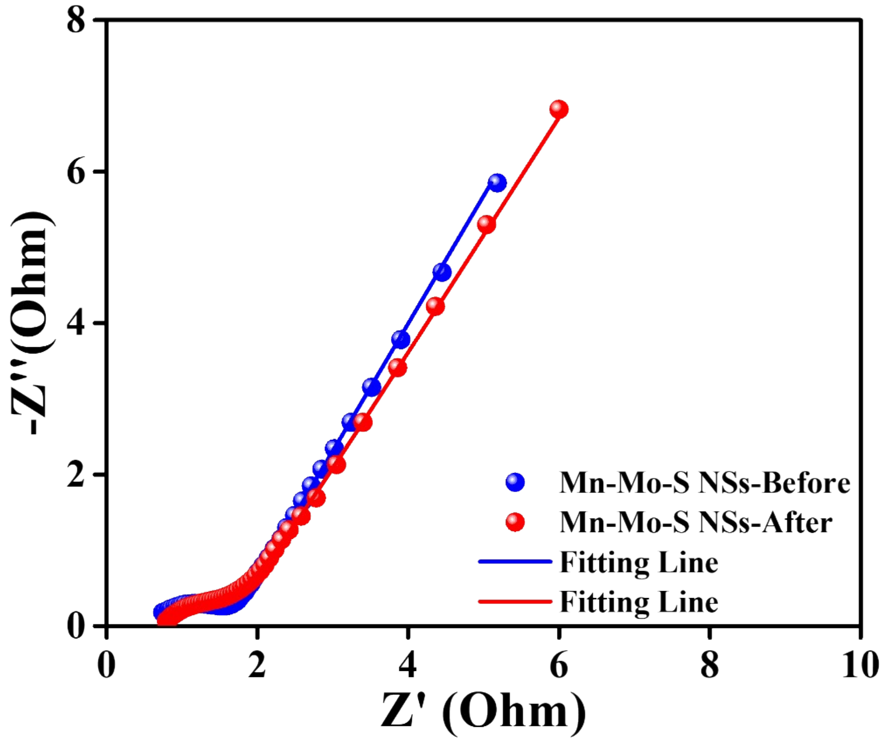

Fig.S11. EIS spectra comparison of Mn-Mo-S NSs-Before and Mn-Mo-S NSs-After.

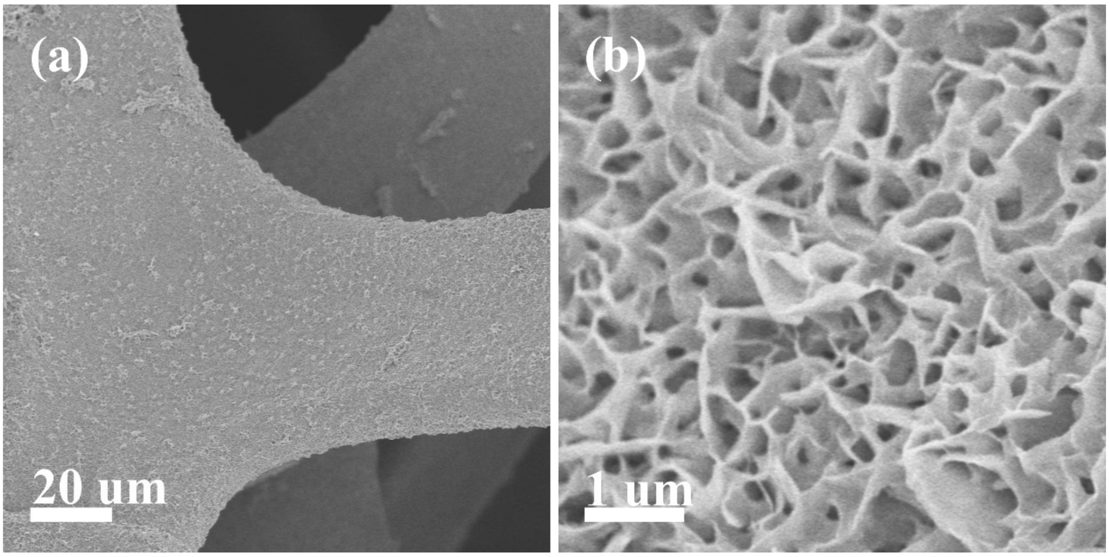

Fig.S12. SEM images for Mn-Mo-S NSs-After.

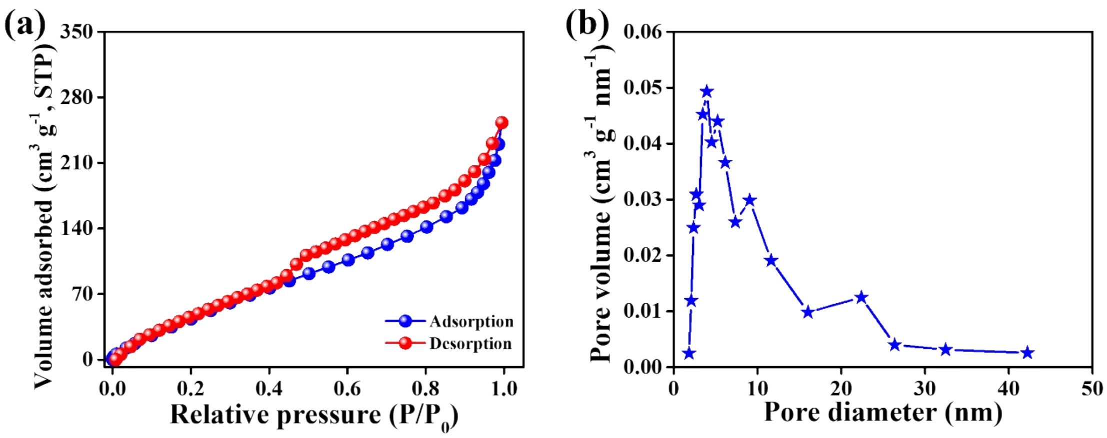

Fig.S13. (a) N_2 adsorption-desorption isotherm and (b) pore size distribution for Mn-Mo-S NSs-After.

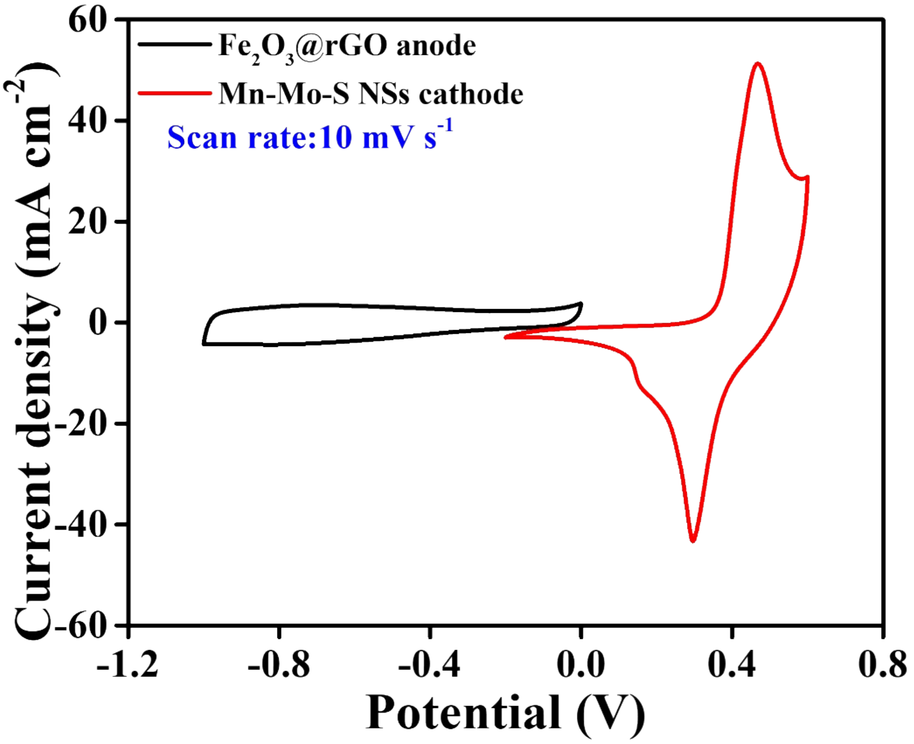

Fig.S14. CV curves of Mn-Mo-S NSs cathode and Fe_2O_3@rGO anode at 10 mV s^{-1}.

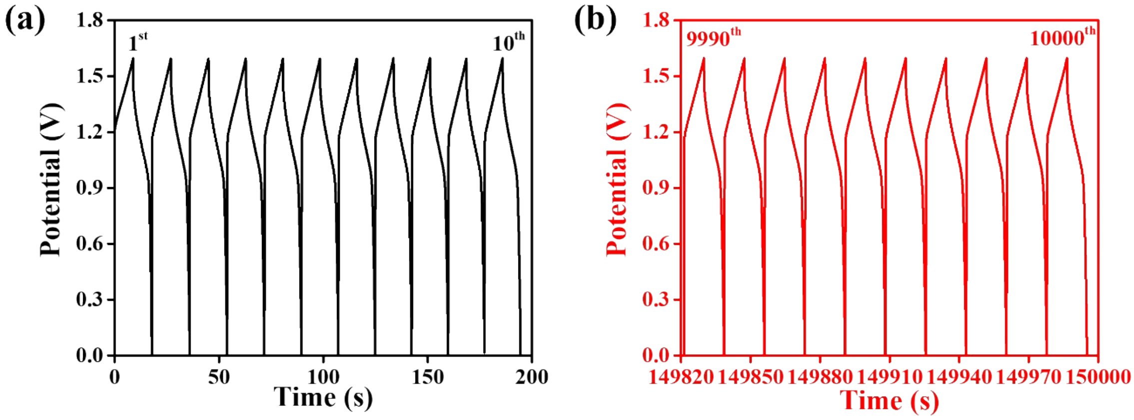

Fig.S15. The initial and final 10 GCD cycles for Mn-Mo-S NSs//Fe_2O_3@rGO HSC in the cyclic stability test at 50 mA cm^{-2} for 10000 GCD cycles.

Table S1. The elemental composition of Mn-Mo-S NSs integrated cathode before and after cycling tests confirmed by the ICP-OES measurements.

Electrode materials	**Mn (at.%)**	**Mo (at.%)**	**S (at.%)**	**O (at.%)**
Mn-Mo-S NSs-Before	12.21	36.72	48.73	2.34
Mn-Mo-S NSs-After	12.13	36.67	47.33	3.87

Table S2. The corresponding electrochemical performance for $MnMoO_4·H_2O$ NS-8 and Mn-Mo-S NSs integrated cathode obtained from the CV data in Fig.S5 and Fig.4a.

Electrode materials	**Scan rate (mVs^{-1})**	**Anodic peak position (V)**	**Anodic peak current (A)**	**Cathodic peak position (V)**	**Cathodic peak current (A)**	**CV integrated area**
$MnMoO_4·H_2O$ NS-8	5	0.449	0.0289	0.315	-0.0258	0.0097
	10	0.471	0.0408	0.301	-0.0368	0.0151
	15	0.484	0.0498	0.291	-0.0447	0.0186
	20	0.497	0.0573	0.282	-0.0511	0.0215
	30	0.509	0.0639	0.275	-0.0565	0.0260
	40	0.518	0.0698	0.269	-0.0613	0.0297
	50	0.536	0.0801	0.259	-0.0696	0.0329
Mn-Mo-S NSs	5	0.446	0.0342	0.309	-0.0291	0.0105
	10	0.467	0.0513	0.298	-0.0432	0.0173
	15	0.485	0.0639	0.288	-0.0532	0.0225
	20	0.499	0.0745	0.281	-0.0614	0.0291
	30	0.52	0.0918	0.268	-0.0745	0.0348
	40	0.536	0.1063	0.258	-0.0854	0.0412
	50	0.555	0.1192	0.248	-0.0947	0.0466

Table S3. The corresponding electrochemical performance for $MnMoO_4 \cdot H_2O$ NSs-8 and Mn-Mo-S NSs integrated cathode obtained from the GCD data in Fig.S6 and Fig.4b.

Electrode materials	Current density ($mA\ cm^{-2}$)	Charge time (s)	Discharge time (s)	Charge capacity ($mAh\ cm^{-2}/mAh\ g^{-1}$)	Discharge capacity ($mAh\ cm^{-2}/mAh\ g^{-1}$)	Rate capability
$MnMoO_4 \cdot H_2O$ NSs-8	2	232.4	231.2	0.14/264.2	0.139/262.3	53.2%
	3	162.6	159.8	0.129/243.4	0.128/241.5	
	5	118.7	113.2	0.115/217	0.114/215.1	
	8	52.1	51.2	0.107/201.9	0.106/200	
	10	34.6	33.3	0.103/194.4	0.102/192.5	
	15	15.7	14.5	0.087/166.1	0.086/164.2	
	20	9.2	8	0.075/141.5	0.074/139.6	
Mn-Mo-S NSs	2	556.8	553.4	0.375/394.7	0.373/392.6	60.6%
	3	319.7	317.4	0.345/363.2	0.344/362.1	
	5	166.4	165	0.29/305.3	0.289/304.2	
	8	89.1	87.5	0.258/271.6	0.257/270.5	
	10	64.2	63.5	0.243/255.8	0.242/254.7	
	15	36.3	35	0.236/248.5	0.235/247.4	
	20	23.4	22.5	0.227/239	0.226/237.9	

Table S4. EIS spectra fitting results for $MnMoO_4 \cdot H_2O$ NSs-8, Mn-Mo-S NSs integrated cathode before and after cycling stability measurements.

Electrode materials	R_s (Ω)	CPE_1-T (mF)	R_{ct} (Ω)	Z_w-R (Ω)	Z_w-T (Ω)	CPE_2-T (mF)
$MnMoO_4 \cdot H_2O$ NSs-8	1.138	0.0053	1.635	6.265	11.62	0.355
Mn-Mo-S NSs-Before	0.763	0.0649	0.838	0.305	2.73	1.598
Mn-Mo-S NSs-After	0.791	0.0376	1.086	0.772	8.66	1.339

Table S5. Electrochemical properties comparison of Mn-Mo-S NSs with recently reported TMSs-type electrode materials in literatures.

Electrode materials	**Areal capacitance/ capacity ($F\ cm^{-2}$/$mAh\ cm^{-2}$)**	**Specific capacitance/ capacity ($F\ g^{-1}$/$mAh\ g^{-1}$)**	**Current load ($A\ g^{-1}$/$mA\ cm^{-2}$)**	**Electrolyte**	**Stability (Cycles)**	**Ref.**
$MnMoS_4$@CNF	-	1727.9 $F\ g^{-1}$	1 $A\ g^{-1}$	3M KOH	84% 6000	1
$FeCo_2S_4$@Ni@Gr	-	390 $mAh\ g^{-1}$	1 $A\ g^{-1}$	3M KOH	58.1% 10000	2
$NiCo_2S_4$/rGO	-	1072 $F\ g^{-1}$	1 $A\ g^{-1}$	6M KOH	-	3
NiCoS@PPy	-	2316.6 $F\ g^{-1}$	1 $A\ g^{-1}$	2M KOH	-	4
rGO/PANI@$NiMoS_4$	-	194 $mAh\ g^{-1}$	0.75 $A\ g^{-1}$	1M KOH	-	5
$NiCo_2S_4$@HCs	-	3178.2 $F\ g^{-1}$	1 $A\ g^{-1}$	2M KOH	95.9% 5000	6
$ZnCo_2S_4$@ppy	-	1486 $F\ g^{-1}$	1 $A\ g^{-1}$	3M KOH	72.9% 5000	7
$MnCo_2S_4$		129.7 $mAh\ g^{-1}$	1 $A\ g^{-1}$	3M KOH	87.81% 4000	8
Ravine-like $MnCo_2S_4$ nanosheets	-	231 $mAh\ g^{-1}$	1 $A\ g^{-1}$	3M KOH	94% 5000	9
NiMn-S	-	2510.15 $F\ g^{-1}$	1 $A\ g^{-1}$	6M KOH	84.5% 5000	10
$CoNi_2S_4$/CNFs	-	1870 $mAh\ g^{-1}$	4 $A\ g^{-1}$	6M KOH	85.1% 5000	11
$ZnGa_2S_4$ hollow spheres	-	358.4 $mAh\ g^{-1}$	2 $A\ g^{-1}$	6M KOH	98.4% 5000	12
Mn-Mo-S NSs	0.373 $mAh\ cm^{-2}$	392.6 $mAh\ g^{-1}$	2 $mA\ cm^{-2}$	2M KOH	96.2% 10000	This work

Table S6. Electrochemical properties comparison with recently reported literatures.

Reported Deviced	**Electrolyte**	**Device Window (V)**	**Energy density (Wh kg^{-1})**	**Power Density (W kg^{-1})**	**Stability (Cycles)**	**Ref.**
$FeCo_2S_4$@Ni@Gr//AC	3M KOH	0-1.6	65.8	849	89.2% 6000	2
$NiCo_2S_4$/rGO//AC	6M KOH	0-1.7	41.52	1067	82% 3000	3
NiCoS@PPy//AC	2M KOH	0-1.6	34.4	799	84% 8500	4
$NiCo_2S_4$@HCs//AC	2M KOH	0-1.6	69.6	847	90.2% 10000	6
$ZnCo_2S_4$@ppy//AC	3M KOH	0-1.6	33.78	800.05	90% 5000	7
$NiCo_2S_4$@$NiMoS_4$//Fe_2O_3/NG	KOH/PVA	0-1.6	72.3	460	90.5% 10000	13
$MnCo_2S_4$ NSs//Fe_2O_3@rGO	KOH/PVA	0-1.6	61.4	244	90.4 % 10000	14
$MnCo_2S_4$/Co_9S_8//AC	6M KOH	0-1.6	45.8	800	94.8% 5000	15
$CoMoS_4$@Ni-Co-S//AC	3M KOH	0-1.6	49.1	800	90.3% 10000	16
MoS_2/$NiCo_2S_4$@C HMSs//AC	6M KOH	0-1.6	53.01	4200	90.1% 10000	17
$MnCo_2S_4$/Co_9S_8//AC	6M KOH	0-1.6	45.8	800	94.8% 5000	18
$NiCo_2S_4$/BPC//BPC	3M KOH	0-1.6	38.5	738.1	89% 4000	19
$NiCo_2S_4$//ARHC	2M KOH	0-1.6	41.1	400	62% 10000	20
$CoMoS_4$/RGO//AC	1M KOH	0-1.5	59.4	1125	99.3% 6000	21
Mn-NiS NSs//ONAC	KOH/PVA	0-1.65	44.2	825	90% 5000	22
$NiCo_2S_4$-Ni_9S_8-C DYMs//rGO gel	6M KOH	0-1.6	51.0	1399.4	84.5% 5000	23
C/$NiCo_2S_4$//AC	6M KOH	0-1.6	34.1	160	78.9% 4000	24
$NiCo_2S_4$/CNT//Fe_2O_3/CNT	3M KOH	0-1.7	41.6	800	82% 5000	25
Mn-Mo-S NSs//Fe_2O_3@rGO	KOH/PVA	0-1.6	72.9	516.8	94.6% 10000	This work

References

1 S. Anand, A. Choudhury, *Mater. Chem. Phys.,* 2023, **299,** 127517.

2 X. Zheng, J. Jiang, T. Bi, F. Jin, M. Li, *ACS Appl. Energy Mater.,* 2021, **4,** 3288-3296.

3 A. I. A. Salam, S. Y. Attia, F. I. E. I. Hosiny, M. A. Sadek, S. G. Mohamed, M. M. Rashad, *Mater. Chem. Phys.,* 2022, **277,** 125554.

4 X. Zhao, Q. Ma, K. Tao, L. Han, *ACS Appl. Energy Mater.,* 2021, **4,** 4199-4207.

5 R. Xiong, X. Zhang, X. Xu, Z. Zhang, X. Tian, C. Wang, *Diam. Relat. Mater.,* 2022, **127,** 109183.

6 J. Zhao, Y. Wang, Y. Qian, H. Jin, X. Tang, Z. Huang, J. Lou, Q. Zhang, Y. Lei, S. Wang, *Adv. Funct. Mater.,* 2023, **33,** 2210238.

7 Y. Wang, C. Xiang, Y. Zou, F. Xu, L. Sun, J. Zhang, *J. Energy Storage,* 2021, **41,** 102838.

8 K. V. G. Raghavendra, C. V. V. M. Gopi, R. Vinodh, S. S. Rao, I. M. Obaidat, H. J. Kim, *J. Energy Storage,* 2020, **27,** 101159.

9 L. Abbasi, M. Arvand, S. E. Moosavifard, *Carbon,* 2020, **161,** 299-308.

10 X. Wang, C. Hao, J. Zhang, C. Ni, X. Wang, Y. Shen, *J. Power Sources,* 2022, **539,** 231594.

11 J. Zhu, C. Han, X. Song, *Mater. Chem. Phys.,* 2022, **283,** 126038.

12 A. M. Zardkhoshoui, M. M. Ashtiani, M. Sarparast, S. S. H. Davarani, *J. Power Sources,* 2020, **450,** 227691.

13 K. R. Shrestha, S. Kandula, N. H. Kim, J. H. Lee, *Chem. Eng. J.,* 2021, **405,** 127046.

14 C. Li, T. Zhao, X. Feng, S. Liu, L. Li, R. Zha, Y. Zhang, Z. Zhang, *J. Alloys Compd.,* 2021, **859,** 157815.

15 H. Jia, J. Wang, W. Fu, J. Hu, Y. Liu, *Chem. Eng. J.,* 2020, **391,** 123541.

16 F. Ma, X. Dai, J. Jin, N. Tie, Y. Dai, *Electrochim. Acta,* 2020, **331,** 135459.

17 Q. Li, W. Lu, Z. Li, J. Ning, Y. Zhong, Y. Hu, *Chem. Eng. J.,* 2020, **380,** 122544.

18 H. Jia, J. Wang, W. Fu, J. Hu, Y. Liu, *Chem. Eng. J.,* 2020, **391,** 123541.

19 J. Feng, X. Zhang, Q. Lu, E. Guo, M. Wei, *Energy Fuels,* 2022, **36,** 5424-5432.

20 Y. Gao, B. Wu, J. Hei, D. Gao, X. Xu, Z. Wei, H. Wu, *Electrochim. Acta,* 2020, **347,** 136314.

21 Z. Zhang, X. Zhang, X. Xu, R. Xiong, X. Tian, C. Wang, *Colloid. Surface. A,* 2022, **652,** 129762.

22 R. K. Devi, M. Ganesan, T. W. Chen, S. M. Chen, M. Akilarasan, S. P. Rwei, J. Yu, T. Elayappan, A. Shaju, *J. Alloy Compd.,* 2023, **944,** 169261.

23 Y. Yan, A. Li, C. Lu, T. Zhai, S. Lu, W. Li, W. Zhou, *Chem. Eng. J.,* 2020, **396,** 125316.

24 W. Lu, M. Yang, X. Jiang, Y. Yu, X. Liu, Y. Xing, *Chem. Eng. J.,* 2020, **382,** 122943.

25 X. Yang, X. He, Q. Li, J. Sun, Z. Lei, Z. H. Liu, *Energy Fuels,* 2021, **35,** 3449-3458.